

Original Articles

Stream network variation in dissolved oxygen: Metabolism proxies and biogeochemical controls



Jacob S. Diamond ^{a,b,*}, Susana Bernal ^c, Amine Boukra ^a, Matthew J. Cohen ^d, David Lewis ^e, Matthieu Masson ^a, Florentina Moatar ^a, Gilles Pinay ^b

^a RiverLy, INRAE, Centre de Lyon-Grenoble Auvergne-Rhône-Alpes, 69100, France

^b Environnement, Ville & Société (EVS UMR5600), Centre National de la Recherche Scientifique (CNRS), Lyon, France

^c Blanes Centre for Advanced Studies (CEAB), Blanes 17300, Spain

^d School of Forest, Fisheries and Geomatics Sciences, University of Florida, Gainesville, FL, USA

^e Department of Integrative Biology, University of South Florida, Tampa, FL, USA

ARTICLE INFO

This article dedicated to Pat Mulholland.

Keywords:

GPP
ER
Primary productivity
Respiration
DOM
Denitrification
Nitrate isotopes

ABSTRACT

An explosion in high frequency dissolved oxygen (DO) observations at river network scales is creating new opportunities to understand dynamic signals in streams and rivers. Among the most informative metrics obtained from DO time series is stream metabolism—comprising gross primary production (GPP) and ecosystem respiration (ER)—but its estimation is non-trivial. There is thus interest in simpler metrics that can capture spatio-temporal patterns in stream metabolism and their consequences for critical ecosystem processes. Using hourly DO time series from 43 agricultural headwater streams reaches (Strahler order 1–5) across five watersheds and two years, we tested the hypothesis that simple DO metrics are useful proxies of stream metabolism, capturing key features of its spatiotemporal variation, and predicting attendant patterns in dissolved organic matter quality and catchment nitrogen processing via denitrification. Our results suggest the diel DO range scaled by stream depth is an excellent proxy for GPP throughout the network, accurately describing its spatial and temporal patterns. In contrast, we found that DO metrics were less successful as proxies for ER, with the maximum daily DO deficit scaled by depth being a good proxy for ER only in higher order streams. We also observed that DO metrics were strongly related to variation in dissolved organic matter quality and denitrification far better than GPP or ER. Finally, we found that DO metrics, GPP, and to a lesser extent ER, had power-law relationships with watershed area (scaling exponents, $\beta = 0.2–0.5$), implying increasing downstream metabolic activity. However, because lower order streams occupy $\sim 75\%$ of network benthic area, total network GPP and ER ($\text{g O}_2 \text{ d}^{-1}$) were disproportionately provided by lower order streams, consistent with recent theoretical modeling. These findings reveal the rich inference space that simple DO metrics can provide, and support their use as proxies for stream metabolism and for inferring network patterns of biogeochemical function.

1. Introduction

Dissolved oxygen (DO) in flowing waters is an information-rich ecosystem indicator, at once integrating energy dynamics, describing aquatic habitat suitability, and constraining biogeochemical processes. Rapid increases in reliability and decreasing costs of in-situ DO sensors (Pellerin et al., 2016; Rode et al., 2016) have enabled freshwater scientists to obtain long time series of high-frequency observations that offer deep insights into inland water functions. A key focus has been on using these DO time series to estimate stream metabolism as the

conjoined fluxes of gross primary production (GPP) and ecosystem respiration (ER) (Appling et al., 2018; Demars et al., 2015; Odum, 1956). Although stream metabolism is a fundamental metric of lotic ecosystems, accurate calculation is non-trivial, especially in headwater and urban streams with noisy DO signals, heterogeneous reaches, and where physical gas exchange (K) with the atmosphere is poorly constrained (Blaszcak et al., 2019). Despite the often dispiriting uncertainties associated with metabolism inferences, much can be learned from simple DO metrics (Moatar et al., 2001; Mulholland et al., 2005; Wang et al., 2003) that obviate the necessity of modeling assumptions

* Corresponding author at: RiverLy, INRAE, 5 rue de la Doua, Villeurbanne 69100, France.

E-mail address: jacob.diamond@inrae.fr (J.S. Diamond).

(e.g., reach homogeneity, constant ER, lack of groundwater inputs) and gas exchange estimates, which are notoriously difficult and uncertain (Demars et al., 2015). Indeed, where broad spatiotemporal patterns are of focal interest, and where the exacting precision of metabolism computations are not required or the assumptions untenable, DO time series attributes may be informative regarding network scale metabolic function.

Network patterns of inland water metabolism have been a central focus of limnology since the emergence of the river continuum concept (Vannote et al., 1980) with modern investigations focused on spatial scaling rules for river networks (Koenig et al., 2019), temporal metabolic regimes (Bernhardt et al., 2018; Savoy et al., 2019), and predictive frameworks (Segatto et al., 2021). Despite the centrality of spatiotemporal network variation to our theoretical understanding of metabolic patterns and their biogeochemical consequences, few studies have empirically evaluated network scale behaviour of metabolism and DO, with those that exist focused primarily on first- and second-order streams (e.g., catchments 0.3–3.7 km² in Mulholland et al. 2005). Exploring how DO and stream metabolism scale in space and time through larger river networks (i.e., up to fifth order streams) thus remains an important knowledge gap.

There are several key predictions of how stream metabolism patterns evolve throughout a headwater stream network. The first prediction, which is borne out of theoretical (Koenig et al., 2019; Vannote et al., 1980) and empirical evidence (Finlay, 2011; McTammany et al., 2003; Mejia et al., 2019), is that GPP increases along river networks as light availability increases with increasing channel widths and reduced shading. This prediction implies that the diel range in DO (sometimes called DO flux, Jankowski et al., 2021 and references therein) increases in similar fashion as light inputs (Wang et al., 2003). In contrast, predictions for how ER may change along a river network diverge. For example, ER magnitude may either 1) stay constant or decrease slightly, or 2) increase along a river network. Empirical evidence for the former derives from studies conducted at the scale of entire river networks from headwaters to mouth (Battin et al., 2008; Hotchkiss et al., 2015), whereas evidence for the latter is found in headwater networks and is attributed to increasing downstream stream temperature (Finlay, 2011; Mejia et al., 2019). Previous efforts have identified maximum daily DO deficits (i.e., the greatest degree of undersaturation) as a reasonable proxy for ER (Mulholland et al., 2005; Wang et al., 2003), implying that this metric should behave similarly to ER throughout the network. Importantly, GPP and ER are scaled from DO concentration changes (g O₂ m⁻³ d⁻¹) to areal fluxes (g O₂ m⁻² d⁻¹) using stream depth (m). Stream depth thus linearly diminishes the resulting DO flux so that for identical GPP or ER, DO diel variation will be greater in headwater than in downstream reaches. Hence, depth corrections of observed DO concentrations are necessary for across order comparisons.

Stream metabolic regimes characterize GPP temporal patterns, integrating primary producer phenology, light availability, timing of resource inputs, and disturbance patterns (Bernhardt et al., 2018). Metabolic regimes are well-predicted by river size because light and temperature tend to increase downstream and larger rivers are less frequently disturbed (Savoy et al., 2019). Further variation around these principal regimes is related to local conditions in turbidity, color, and disturbance which can lead to asynchronous behavior across river networks (Mejia et al., 2019; Roberts et al., 2007), and high within-network variability. How DO signals relate to these network properties remains an open question, especially in disturbed systems (Blaszcak et al., 2019), but temporal patterns in simple DO metrics may prove to be useful in characterizing metabolic regimes, even where metabolism assumptions are untenable.

Stream metabolic rates and associated DO patterns are linked to both dissolved organic matter (DOM) and nitrogen (N) processing by stream biota. For instance, DOM derived from GPP tends to be richer in aliphatic structures than allochthonous-derived DOM (Hansen et al., 2016; Helms et al., 2008; Zhang et al., 2013). On the other hand,

consumption of DO, and therefore minimum daily concentrations, is controlled by biological respiration and decomposition of organic matter that tends to decrease DOM molecular weight (Hansen et al., 2016; Helms et al., 2008; Zhang et al., 2013). In turn, large DO deficits affect the balance between oxic and anoxic respiration pathways, and are therefore linked to increased potential for in-stream denitrification (Christensen et al., 1990), which requires low DO. This process integration of oxygen, DOM quality, and denitrification suggests that changes in DO concentrations along the stream should both control and result from in-stream biogeochemical processes and by-products.

Here, we used spatiotemporal variation in DO signals along an agricultural headwater stream network to evaluate simple inferences of spatial and temporal variation in metabolic rates, and as predictors of key biogeochemical processes. We hypothesized that metrics based on diel variations in DO concentrations would be robust proxies of stream metabolism, and thus, could qualitatively capture temporal and spatial variation of metabolic activity. In addition, we hypothesized that DO metrics would be informative of network patterns of biogeochemical processes strongly linked to stream metabolism and DO availability such as in-stream DOM cycling and denitrification. Thus, we expected strong relationships between DO proxies of stream metabolism and both DOM quality and denitrification isotopic N signatures.

2. Methods

2.1. Study area

We studied 43 stream sites ranging from Strahler order 1 to 5 within five agricultural watersheds in the Forez plain of the Loire River, France from July 2019–October 2020 (Fig. 1). The study area in the headwaters of the Loire comprises a valley uplifted during the Tertiary and glaciated during the Quaternary, bound by the Monts du Lyonnais to the east and the Monts du Forez to the west, with sites spanning an elevation gradient of 330 to 627 m.a.s.l. (NGF IGN69 datum). Lithology near the Loire River at watershed outlets is typically a thick alluvium with clay and sand derived from granite and gneiss rocks. Higher in the watersheds, lithology is typically granite and gneiss. Topography is characterised by rolling hills with successions of plateaus separated by long steep slopes. Drainage networks are dense and valleys are deeply incised. Climate in the Forez plain is continental, with mean annual rainfall of approximately 800 mm, and mean annual temperatures of 11 °C (mean annual minimum–maximum = 6.1–17.2 °C). This area has been continuously occupied since at least 5750 cal. BP with agricultural activity, damming, and water mills growing throughout the Iron Age and Gallo-Roman period around 2000 cal. BP (Cubizolle et al., 2012, 2003; Georges et al., 2004).

2.2. Data collection

We monitored all sites for DO (g m⁻³) and temperature (°C) every 15 min and supplemented these data with seasonal grab samples of water chemistry (up to 5, depending on site) between July 2019 and October 2020, (Fig. 2); we did not collect DO and temperature data during winter (November–February). At each site, DO and temperature were measured with an *in-situ* sensor (HOBO U26-001, Onset Computer Corporation, Massachusetts, USA) instrumented with a copper anti-biofouling guard. We cleaned these sensors every two weeks to remove biofouling. Prior to deployment, we lab-calibrated DO sensors with both 100% water-saturated air and with sodium sulphite for 0% saturation. We also measured DO and temperature with a calibrated handheld probe (Pro Plus, YSI Inc., Ohio, USA) at each field visit to check for sensor drift and develop corrections as needed. We placed sensors in the middle of the water column, and as close to the thalweg as possible; sites downstream of confluences were placed at least 20 stream widths downstream to ensure mixing (Siders et al., 2017).

For use in metabolism modeling, we gathered meteorologic and

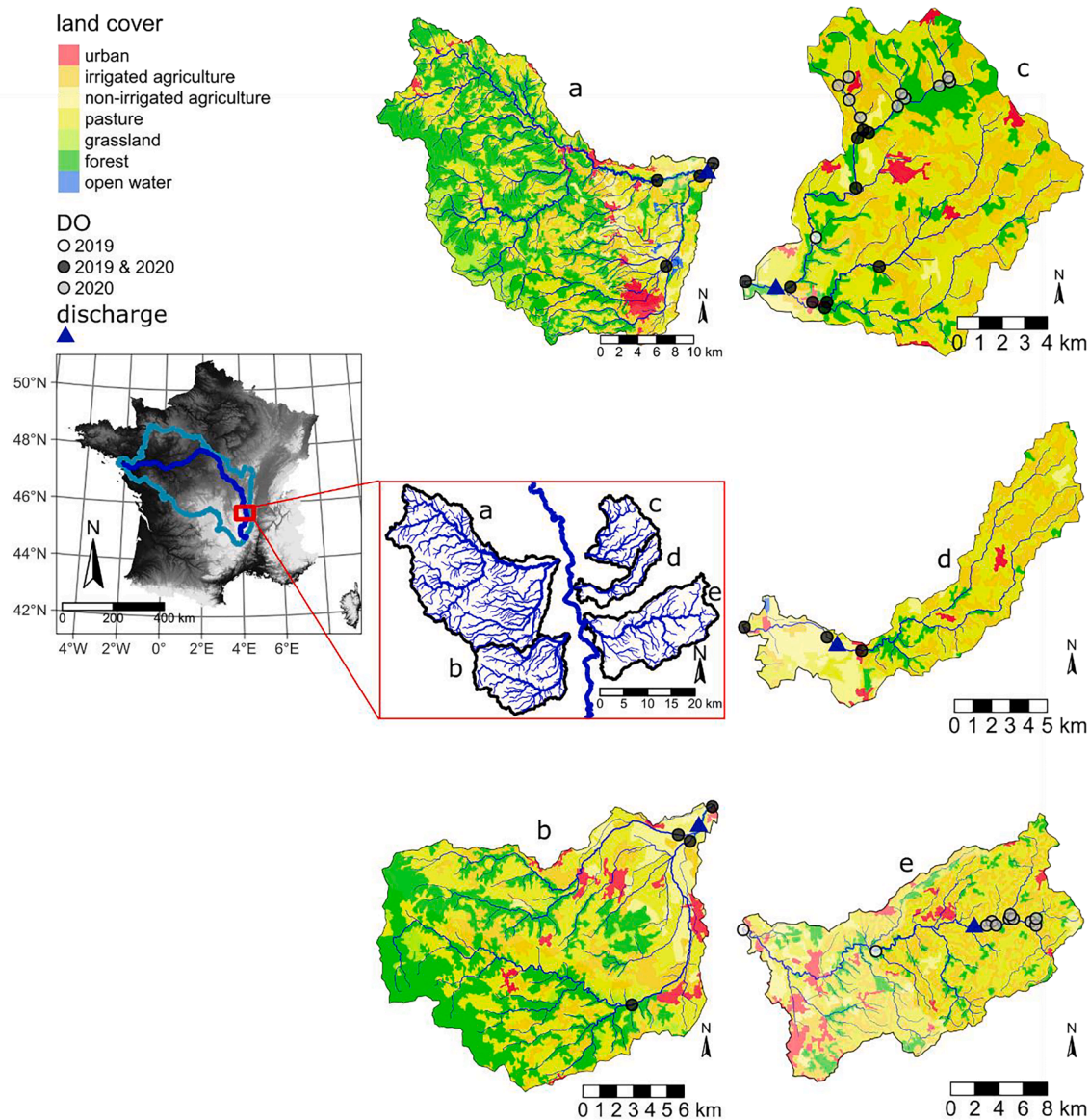


Fig. 1. Map of the 43 stream sites measured for dissolved oxygen concentration (DO), temperature, and water chemistry across five watersheds (letters matched in inset to aid in identification) in the headwaters of the Loire River (heavy dark blue line), France (inset shaded by elevation above sea level) and Loire River watershed shown. Corinne land cover classes shown for each watershed (their location with respect to the main stem is shown in the red-bordered inset). Stream sites are coloured according to the timing and length of the measurement period for DO and discharge measurement sites are shown with blue triangles. (For interpretation of the references to color in this figure legend, the reader is referred to the web version of this article.)

hydraulic data from several sources. First, we obtained hourly atmospheric pressure (kPa), insolation (W m^{-2}), and rainfall (mm) data from Météo France at the nearby St. Etienne-Bouthéon station (site 42005001; <https://publitheque.meteo.fr/>). We then obtained instantaneous discharge ($\text{m}^3 \text{s}^{-1}$) data for one downstream location in each of the five watersheds from the French Banque Hydro database (<http://hydro.eaufrance.fr/>; Table 1) and assumed the same specific discharge (q [mm d^{-1}]) across all sites in the same watershed. Daily discharge at each site was therefore the q for its watershed multiplied by site drainage area. Stream depth was modeled at each site by first mapping each site location to its corresponding stream reach from an empirical reach-based hydraulic geometry model for France (Morel et al., 2020). Model inputs were daily discharges estimated at each site (see above), and model outputs included daily values of stream depth (m), velocity (m s^{-1}), and width (m) for the model reach of each site. For the modeled region, depth estimates are accurate (RMSE = 1.9 cm) and unbiased

(bias = +0.6 cm) compared to observations ($n = 203$; Morel et al. 2020). We estimated stream surface light availability using a physical model of water temperature ("TNET") for the Loire River network that operates on the same reaches as the hydraulic model (Beaufort et al., 2016). The TNET model outputs hourly shade (unitless) for each reach depending on riparian vegetation density, riparian tree height, riparian tree phenology, solar angle, and azimuth. There are no validation data for the shade outputs, but the model had high agreement ($R^2 = 0.90$) with observations in its original development (Li et al., 2012).

To evaluate variation in biogeochemical function and assess the explanatory power of DO metrics and metabolism, we took stream water grab samples of DOM quality and stable isotopes of NO_3^- ($N = 156$, $n = 2-5$ per site) in five different seasons (Fig. 2, numbered arrows). We characterized DOM molecular features such as aromaticity and weight, as these properties reflect DOM source and regulate respiration. Specifically, we measured ultraviolet-visible (200–800 nm) spectroscopy

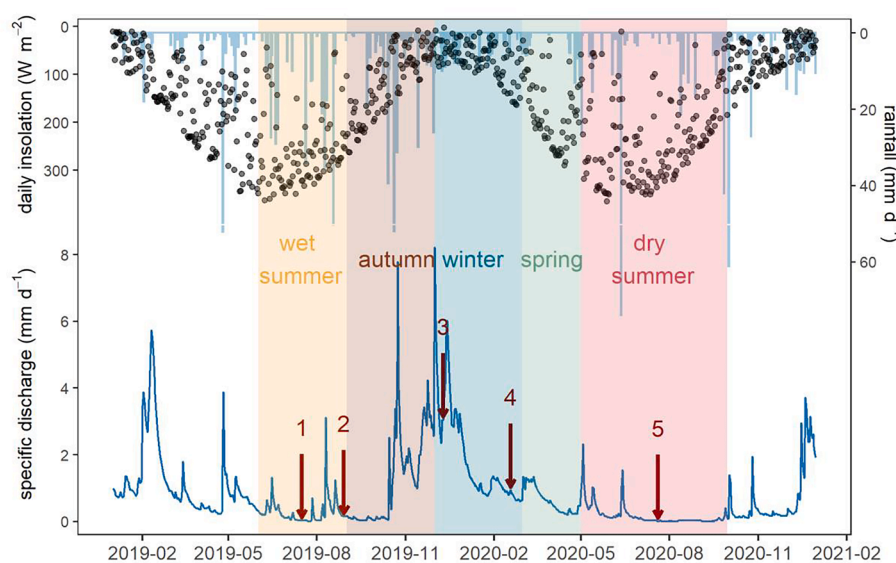


Fig. 2. Representative daily hydroclimatic conditions showing discharge (blue line), insolation (black dots), and precipitation (blue vertical bars) in the Coise catchment (site code = K0663310) during monitoring period. Specific discharge was assumed to be the same for all sites within each watershed. Timing and magnitude of q shown here was similar across watersheds. The five study periods (wet summer, autumn, winter, spring, and dry summer) are denoted with shaded color bands. Red arrows indicate grab sampling events. (For interpretation of the references to color in this figure legend, the reader is referred to the web version of this article.)

Table 1

Drainage area range and number of study sites in each watershed (n), discharge code*, N surpluses** (mean \pm sd), and riparian land use[†] within a 100 m linear upstream buffer[‡] of each site (mean \pm sd) by watershed.

| Watershed | Area (km ²) | Discharge site code | N surplus (kg ha ⁻¹ y ⁻¹) | Crops (%) | Pasture (%) | Forest (%) | Urban (%) |
|-----------|-------------------------|---------------------|--|-------------|-------------|-------------|------------|
| Loise | 1–132 (n = 21) | K0714010 | 31.5 \pm 14.1 | 8 \pm 6 | 59 \pm 27 | 37 \pm 25 | 6 \pm 5 |
| Toranche | 55–76 (n = 3) | K0704510 | 46.0 \pm 16.8 | 51 \pm 8 | 19 \pm 3 | 24 \pm 13 | 7 \pm 2 |
| Coise | 6–305 (n = 11) | K0663310 | 57.7 \pm 25.4 | 8 \pm 5 | 80 \pm 14 | 25 \pm 15 | 16 \pm 5 |
| Lignon | 62–664 (n = 4) | K0773220 | 16.8 \pm 3.8 | 27 \pm 22 | 27 \pm 18 | 61 \pm 30 | 0 \pm 0 |
| Mare | 62–233 (n = 4) | K0643110 | 17.8 \pm 4.1 | 60 \pm 42 | 14 \pm 9 | 27 \pm 25 | 7 \pm 4 |

*Banque Hydro site codes.

**CASSIS–N database (Poisvert et al., 2017), <https://geosciences.univ-tours.fr/cassis>.

[†]2018 CORINE dataset (CLC 2018).

[‡]Buffers are 100 m wide on both sides of the upstream stream reach length defined for each site

(UV-vis) of DOM with Shimadzu UV-1900 spectrophotometer (Shimadzu Scientific Instrument, Inc., Columbia, MD, USA) at three periods: wet summer, low winter flow, and dry summer (Fig. 2). Prior to analysis, samples were filtered through 0.45 μ m polyvinylidene fluoride membranes. We calculated the following UV-vis metrics: 1) specific UV absorbance at 254 nm (SUVA in L mg C⁻¹ m⁻¹), the absorbance at 254 nm normalized by DOC concentration (Weishaar et al., 2003), 2) E4:E6, the ratio of absorbances at 400 and 600 nm, 3) E2:E3, the ratio of absorbances at 250 nm and 365 nm, and 4) spectral slope (S_R), the ratio between absorbance slopes (in natural log units) for the wavelength regions 275–295 nm and 350–400 nm (Helms et al., 2008). Briefly, SUVA is positively correlated with DOM aromaticity (Weishaar et al., 2003), E4:E6 and E2:E3 are negatively correlated with aromaticity and molecular weight (Li and Hur, 2017), and S_R is negatively correlated with molecular weight but positively with irradiation (Helms et al., 2008).

Finally, we measured the isotopic composition of N and O in NO₃[–] (¹⁵N-NO₃[–] and ¹⁸O-NO₃[–], respectively) with the bacterial denitrification method (*Pseudomonas chlororaphis* subsp. *aureofaciens*; Casciotti et al., 2002; Sigman et al., 2001; GasBench-PreCon-IRMS, UC Davis, USA) for four grab sample sets: wet summer, high winter flow, low winter flow, and dry summer (Fig. 2). Prior to sample analysis, we removed nitrite from our samples by acidifying with sulfamic acid and then neutralizing with sodium hydroxide (Granger and Sigman, 2009). Isotopic results are presented in delta notation as $\delta^{15}\text{N-NO}_3^-$ (‰) and $\delta^{18}\text{O-NO}_3^-$ (‰) relative to international standards. Mean standard deviations of analytical sample replicates were half ($sd_{\delta^{15}\text{N}} = 0.11\%$; $sd_{\delta^{18}\text{O}} = 0.13\%$) that of mean standard deviations of reference replicates ($sd_{\delta^{15}\text{Nair}} = 0.23\%$; $sd_{\delta^{18}\text{OVSOW}} = 0.26\%$).

2.3. Data processing

Prior to analysis, we conducted quality control on the DO data (n = 986,349). We first averaged DO data to hourly resolution to reduce file sizes and processing time (n = 246,947), and then flagged data that were extremely noisy or otherwise of suspect quality (e.g., negative values, sensor out of the water), reducing sample size by 4%. We then compared *in situ* sensor measurements to hand-held probe observations and removed data where clear, uncorrectable sensor drift, sensor burial, or biofouling had occurred, accounting for approximately 6% of the remaining data. Finally, when *in situ* and hand-held observations disagreed (n = 10 cases), but indicated linear drift, we corrected these data with a linear model ($p < 0.001$), influencing approximately 1% of the data. For data that passed quality control (n = 222,339), we calculated hourly DO saturation (DO_{sat}) using water temperature and barometric pressure at sea level corrected for site elevation, and derived hourly DO saturation deficit (=DO minus DO_{sat}), with a negative deficit indicating measured DO is below saturation. We calculated four daily DO metrics for each site as potential proxies of stream metabolism following the logic of Mulholland et al. (2005) and Wang et al. (2003):

1. Daily DO range (g m⁻³), measured between 04:00 and 03:00 the next day, in solar time (i.e., solar noon is always 12:00).
2. Maximum DO deficit (g m⁻³), defined as the greatest negative departure from DO_{sat} in each 24-hr period; values were negative for 98% of days.
3. Daily DO range multiplied by daily average water depth (g m⁻²), to account for depth dependency (vis-à-vis benthic surface area to volume effects).

4. Maximum DO deficit multiplied by the daily average water depth (g m⁻²).

2.4. Stream metabolism modeling

We estimated stream metabolism at each site using a single-station open channel method (Odum, 1956). The approach is a mass-balance representation of DO as a function of insulation-dependent inputs from GPP (g O₂ m⁻² d⁻¹), constant ER (g O₂ m⁻² d⁻¹), and temperature- and concentration-dependent gas exchange (K₆₀₀ [d⁻¹]) between the water and air. We simultaneously estimated GPP, ER, and K₆₀₀ using inverse fitting of DO dynamics with a state space approach (i.e., including process and observation error) and Bayesian inference with Markov chain Monte Carlo sampling (MCMC) (Appling et al., 2018). We developed site-specific hyperpriors for K₆₀₀ as lognormal distributions of the daily means from equations 1, 3, 4, and 5 Raymond et al. (2012), which relate K₆₀₀ to velocity, slope, and depth. We then constrained K₆₀₀ by pooling its estimates based on site-specific discharge, where days with similar discharge are more likely to have similar K₆₀₀; this corresponds to the *b_Kb_oipi_tr_plrckm.stan* model in the *streamMetabolizer* R package (version 0.10.9) (Appling et al., 2018). Four MCMC chains were run in parallel on four cores, with 1000 warmup steps and 500 saved steps on each chain. We evaluated model fits with the Gelman-Rubin convergence diagnostic, R (Gelman and Rubin, 1992), ensuring that all parameters had an R value less than 1.1 (Brooks and Gelman, 1998). When this criterion was not met, indicating poor MCMC model convergence, we excluded metabolism estimates from further analyses. Model outputs included daily posterior probability distributions for GPP, ER, K₆₀₀. We used the means of these distributions as the best daily estimates, the variances as uncertainty measures, and the 95% credible intervals (Bayesian confidence intervals) to test if the estimates were the correct sign (i.e., GPP > 0, ER < 0).

2.5. Data analyses

We evaluated proposed DO metrics as prospective proxies of GPP and ER by comparing 1) DO diel ranges (with and without depth scaling) to estimated daily GPP, and 2) maximum daily DO deficits (with and without depth scaling) to ER at each site. To do so, we used: 1) an iteratively reweighted least squares regression (IRLS), 2) multiple regression with Strahler order as a second fixed effect. By accounting for Strahler order, we were able to test if there were predictable network scale effects on the efficacy of the potential proxies. Residuals from model fits were normal and homoscedastic, but did exhibit autocorrelation. However, model performance was not improved using autocorrelated variance structures, so we opted to keep the models simple. To simplify interpretation of all analyses, we used absolute values of ER and maximum daily DO deficit. All statistical analyses were performed in R (R Core Team, 2020).

We evaluated the coherence of metabolism and DO proxy patterns through the fluvial network with log-log linear regression of site means versus watershed area. Log-log regression relates relative, not absolute, changes in variables, and thus allows comparison of area scaling effects on metabolism and DO proxies (via comparison of power-law slopes), providing direct assessment of the coherence of their spatial patterning. To compute means of metabolic rates, we used inverse variance weighting to account for uncertainty in metabolism measurements such that measurements of GPP or ER with greater uncertainty were assigned lower weights. Means of DO proxies were simple averages. We compared regression slopes of DO proxies and metabolism (seasonally and annually) against watershed area, and considered them equal if their 95% confidence intervals overlapped.

We evaluated whether DO proxies captured the temporal regimes of metabolism using Kendall τ correlation and visual inspection. We compared mean weekly values (weeks 10–44) across sites within each Strahler order (orders 1–5) to account for any scale-dependence of (i.e.,

effects of watershed area on) temporal patterns. Similar to our spatial analysis, we used weighted means for stream metabolic rates (GPP and ER), simple means of DO proxies, and absolute values of ER and maximum daily DO deficit. We calculated Kendall τ values and their respective p-values for relationships between 1) GPP and diel DO range \times depth, and 2) |ER| and |maximum daily DO deficit| \times depth. When p-values < 0.05 and $\tau > 0.2$, we considered the two time-series to have the same temporal regime.

Finally, we evaluated the relative performance of DO metrics and metabolism estimates for predicting variation in stream C quality and N processing using regression and Spearman correlation. We correlated mean daily DO metrics and metabolism (GPP and ER) with DOM UV-vis properties and NO₃⁻ stable isotope values from grab samples. For DO proxies and metabolism, we used the mean of the three prior days to the grab sample date (including day of sampling, n = 3). Specifically, we calculated IRLS and Spearman correlations (ρ) of a) DO proxies (with and without depth-scaling) and b) metabolism with 1) DOM UV-vis metrics indicative of aliphatic vs. aromatic compounds (E4:E6, SUVA, E2:E3) and molecular weight (S_R), and 2) indicators of in-stream denitrification (enriched $\delta^{15}\text{N}$ and $\delta^{18}\text{O}$ of NO₃⁻).

3. Results

3.1. General observations for DO and stream metabolism

We observed seasonal variation in DO concentration patterns through the river network. Larger streams exhibited daily means more consistently near saturation than smaller streams, except in spring (Fig. 3a). In the spring, diel DO ranges and DO deficits increased with stream order, but these patterns were not consistent throughout the year (Fig. 3a). During the wet summer and autumn, lower order streams exhibited greater DO deficits than higher order streams, but diel DO ranges were similar throughout the network (Fig. 3a). In contrast, during the dry summer (with lower q; Fig. 3b), low order streams exhibited larger diel DO ranges than large streams, but much higher average DO deficits.

Across sites and seasons, estimated GPP ranged from 0.1 to 4.3 g O₂ m⁻² d⁻¹ (0.7 ± 0.6 g O₂ m⁻² d⁻¹, mean \pm sd) and estimated ER ranged from -0.5 to -21.0 g O₂ m⁻² d⁻¹ (-4.0 ± 2.2 g O₂ m⁻² d⁻¹). Notably, credible intervals for ER (2.6 ± 1.5 g O₂ m⁻² d⁻¹, mean \pm sd) were 3–4 times the width of intervals for GPP (0.7 ± 0.4 g O₂ m⁻² d⁻¹), with the greatest discrepancies in autumn, indicating poorly constrained estimates. Days with successful metabolism estimates varied widely by site (114 ± 64 days, range = 4–241 days, overall n = 8,800 site-days). There were $69 \pm 18\%$ fewer days with metabolism estimates than the total DO data available. Data losses resulted from poor model fits, with Gelman-Rubin R values for parameters greater than 1.1 (indicating poor model convergence) 12% of the time, and incorrect signs for estimated GPP and ER 54% of the time. We also observed obvious equifinality in ER estimates as indicated by ER covariance with K₆₀₀ (Appling et al., 2018) (Fig. S1a). Poor estimates occurred principally in smaller order streams, and on days when DO signals were noisy, especially during drying periods in the summer or storm events. Overall, K₆₀₀ was well within the range of reported values in the literature (Raymond et al. 2012) for streams of this size range (median = 11.9 d⁻¹; interquartile range = 6.6–23 d⁻¹), and correlated positively with discharge, particularly in spring (Fig. S1b).

3.2. Simple DO metrics as proxies of stream metabolism

When data were pooled across sites and dates, both DO range metrics (with and without depth scaling) were strongly correlated with stream GPP estimates (Fig. 4a,b). Depth-scaled DO diel range yielded the strongest relationship, explaining 70% of estimated variation in GPP according to the IRLS model (Fig. 4b). Goodness-of-fit was marginally improved by considering the interaction effect of Strahler order ($R^2_{\text{adj}} =$

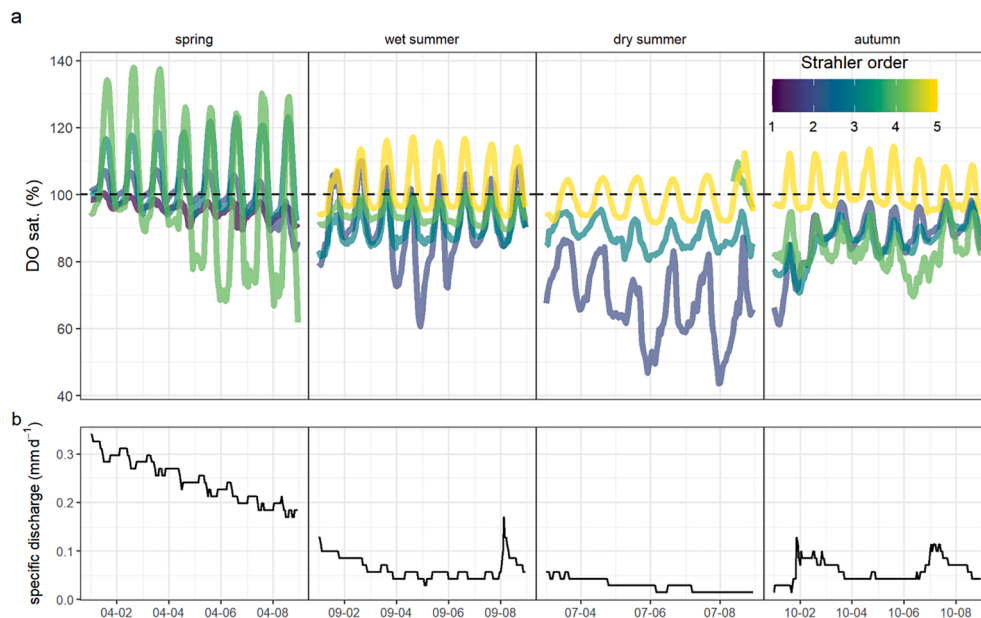


Fig. 3. Network patterns of stream DO and discharge for exemplary periods across seasons. a) Hourly DO in percentage saturation averaged across all sampled reaches ($n = 43$) within their respective Strahler orders (for Strahler orders 1–5, $n = 4, 11, 16, 8$, and 3, respectively); dark colors are the lowest Strahler orders and light colors are higher Strahler orders. The dotted line shows 100% percent saturation. b) Exemplary hourly q in the Coise catchment for each season; other catchments exhibited similar patterns and magnitude. Winter data were not collected.

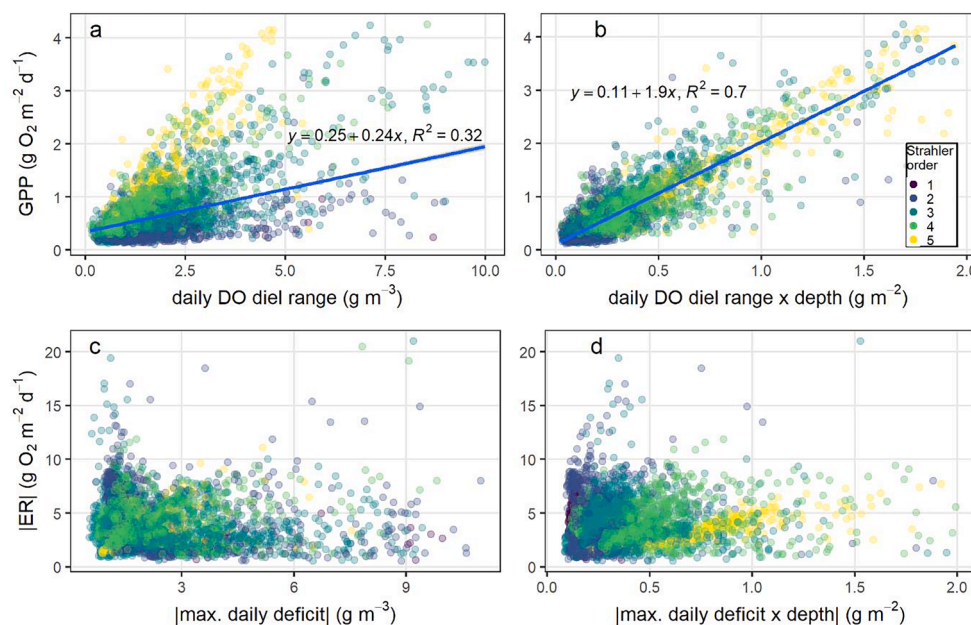


Fig. 4. Gross primary production (GPP) and ecosystem respiration (ER) (expressed in absolute terms) versus DO metrics for all days when stream metabolism could be estimated. a) GPP versus daily diel DO range and b) same relationship as in a) accounting for depth effects on the DO metric; c) ER versus maximum daily DO deficit (expressed in absolute terms) and d) same relationship as in c) accounting for depth on the DO metric. Colored circles indicate different stream Strahler orders. The blue line is the linear regression obtained with the IRLS model across-sites; the corresponding equation and goodness-of-fit (adjusted R^2) are shown in each case where $p < 0.05$. (For interpretation of the references to color in this figure legend, the reader is referred to the web version of this article.)

0.73), although none of interaction effects were different from each other ($p = 0.05$; Table 2)

Ecosystem respiration was uncorrelated with the daily maximum DO deficit metrics, regardless of depth scaling (Fig. 4c,d). However, the goodness-of-fit was improved by considering the fixed interaction effects of Strahler order ($R^2_{\text{adj}} = 0.09$), showing a large directional increase in both slope and intercept with Strahler order (Table 2). This is visually apparent as well in the horizontal sorting of Strahler orders in the ER–daily max. DO deficit relationship (Fig. 4d).

3.3. Spatial patterns of DO and stream metabolism

Spatial patterns of stream metabolism were similar to those of DO metrics, in many cases increasing with watershed area (Figs. 5 and 6). When scaled by depth (blue points, Figs. 5 and 6), DO metrics exhibited strong spatial coherence with GPP estimates during most seasons as

indicated by nearly identical best-fit slopes (β). This was true for the diel DO range metric across all seasons, and for the maximum daily DO deficit metric during the dry summer and, to a lesser extent, autumn. When metrics were not depth-corrected (red points, Figs. 5 and 6), their spatial patterns were at times inverted to estimated metabolic patterns, with the exception of the diel DO range in spring. We observed that the magnitude of depth-indexed daily DO range (Fig. 5a–d) and maximum daily DO deficit increased with stream order (Fig. 6a–d), a finding that was consistent across seasons. Moreover, the slopes of these increases were similar between the two metrics. This pattern emerged largely because depth increased with increasing watershed area ($\ln(\text{depth}) = \ln(\text{area})^2, \beta = 0.27 \pm 0.02, R^2 = 0.88, p < 0.001$), such that, for a similar DO concentration, DO mass increases with distance downstream. For the depth-scaled maximum DO deficit, a consistent trend of increasing magnitude with area contrasted with both the absence of any clear pattern (spring and wet summer), and the decreasing magnitude (dry

Table 2

Multiple regression results for metabolism fluxes versus DO metrics ($n = 3823$). The GPP and ER columns separate the two model response variables, with scaled model parameter estimates (confidence interval) and their p-values reported. GPP models relate GPP to daily diel range \times depth with a Strahler order interaction and ER models relate maximum daily DO deficit \times depth with a Strahler order interaction.

| Predictors | GPP | | ER | |
|--------------------------|--------------------|------------------|-------------------------|------------------|
| | Estimates | p* | Estimates | p |
| (Intercept) | 0.23 (0.11–0.34) | <0.001 | 5.34 (4.56–6.12) | <0.001 |
| DO metric \times depth | 1.12 (0.27–1.98) | 0.010 | -7.24 (-11.79 to -2.70) | 0.002 |
| strahler [2] | 0.02 (-0.10–0.14) | 0.710 | -1.08 (-1.88 to -0.27) | 0.009 |
| strahler [3] | -0.08 (-0.20–0.04) | 0.196 | -1.79 (-2.59 to -0.99) | <0.001 |
| strahler [4] | 0.04 (-0.09–0.16) | 0.564 | -1.96 (-2.78 to -1.13) | <0.001 |
| strahler [5] | 0.07 (-0.06–0.19) | 0.296 | -3.71 (-4.56 to -2.85) | <0.001 |
| DO * strahler [2] | 0.10 (-0.76–0.97) | 0.814 | 8.05 (3.46–12.65) | 0.001 |
| DO * strahler [3] | 0.75 (-0.11–1.60) | 0.086 | 7.92 (3.34–12.49) | 0.001 |
| DO * strahler [4] | 0.33 (-0.52–1.19) | 0.446 | 8.73 (4.16–13.29) | <0.001 |
| DO * strahler [5] | 0.40 (-0.45–1.25) | 0.358 | 9.38 (4.82–13.94) | <0.001 |
| R ² adj | 0.73 | | 0.075 | |

*p-values less than 0.05 are bolded.

summer and autumn) observed when depth adjustments were not considered. This was also true for daily DO diel ranges.

Stream GPP consistently increased with watershed size during all seasons, with an order of magnitude difference between the smallest and largest streams (Fig. 5e-h). Across seasons, GPP increased by 0.28–0.52 % for every 1% increase in watershed area (power law slopes), with the greatest increases in spring. This is likely due to increasing light availability at the stream surface in larger streams (Fig. S2). Stream ER showed no consistent pattern with increasing watershed size (Fig. 6e,f), except during the dry summer of 2020 and autumn when ER increased by 0.13–0.2% for every 1% increase in watershed area (Fig. 6g,h). Log-

log slopes were all less than one, indicating marginal watershed size effects on GPP and ER with increasing watershed size.

3.4. Temporal patterns of DO and stream metabolism

Temporal alignment of stream metabolism and DO metrics depended strongly on Strahler order (Fig. 7). GPP and depth-scaled diel DO range were most temporally aligned, with strong correlations ($\tau > 0.2$) in Strahler orders 2–5 (Fig. 7a–e). In Strahler orders 1 and 2, GPP was relatively constant over the year, whereas in orders 3 and 4, GPP peaked in spring and declined nearly an order of magnitude over the remaining growing season; GPP signals in order 5 exhibit a weak summer peak, though our record is shorter. In contrast, ER and maximum daily DO deficit \times depth, were inversely correlated for Strahler orders 1–3, and only exhibited temporal coherence in Strahler order 4 (Fig. 7f–j). Maximum daily DO deficit \times depth was the most temporally dynamic of the metrics, increasing an order of magnitude from spring to summer, where they could then remain constant, increase, or decrease from summer to autumn. ER temporal patterns contrasted with those for GPP, decreasing over summer, but exhibiting spring and autumn peaks, especially in orders 2–5 (Fig. 7f–j).

3.5. DO metrics and in-stream C and N biogeochemical processing

DOM characteristics differed across sampling campaigns (Table 3; Fig. 8), with wet and dry summers differing on every UV-vis metric ($t_{22-52} = -25.6$ –11.1, $p < 0.001$). Of particular note was our observation that dry summer DOM was more similar to winter than to wet summer DOM (Table 4 and Fig. 8c,f), with winter and dry summer exhibiting no difference in E2:E3 ($t_{62} = -1.6$, $p = 0.15$) or E4:E6 ($t_{47} = -0.3$, $p = 0.76$), and only modest differences in S_R ($t_{35} = -3.7$, $p = 0.002$) and SUVA ($t_{75} = -3.2$, $p = 0.01$) (Table 4).

DO metrics consistently outperformed metabolism estimates in predicting variation in DOM quality (Fig. 8). The E4:E6 index of aliphatic structure increased with increasing daily DO diel range \times depth, but was uncorrelated with GPP, especially during the wet summer (blue circles, Fig. 8a). Likewise, GPP exhibited no correlation with E4:E6 patterns during the wet summer, and yielded equivalent predictions as the DO metric during the dry summer (red circles; Fig. 8b). S_R (an indicator of molecular weight) correlated far more strongly with maximum daily DO deficit (Fig. 8d) than with ER (Fig. 8e) in the dry summer, but was

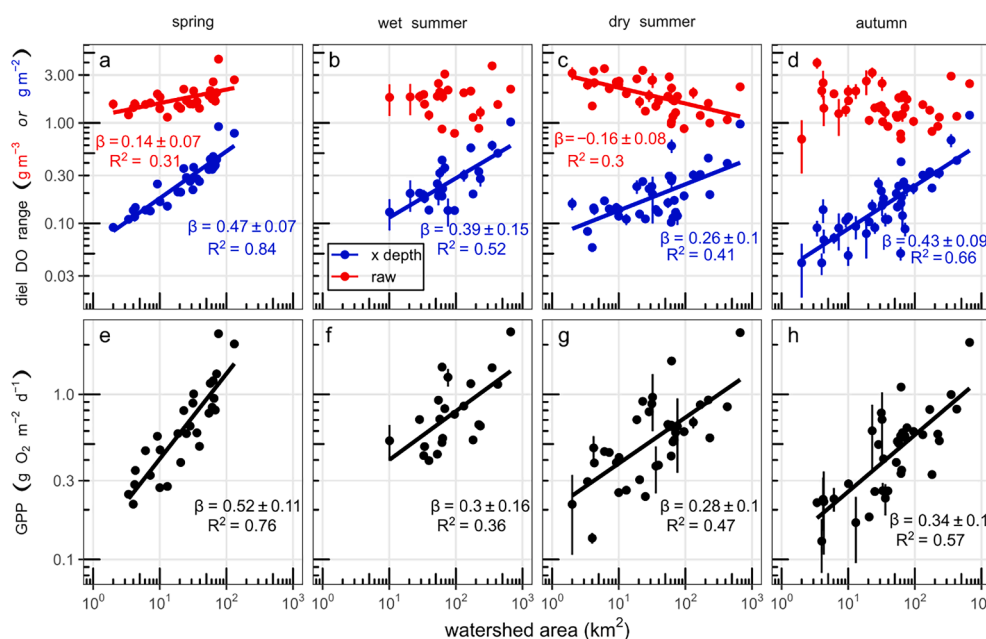


Fig. 5. Spatial patterns in mean daily GPP and mean diel DO range by season and watershed area. a–d) Red points are raw values of diel DO range and blue points are indexed by stream depth (note change in units on y-axis). e–h) GPP follows a nearly identical spatial pattern to diel DO range \times depth. Vertical bars indicate standard errors; note that many SE values smaller than the plotted point. Best fit lines are ordinary least square regressions and text indicates slope coefficients \pm 95% confidence intervals and coefficients of determination (R^2); best fit lines only shown for $p < 0.05$. Note log-log scale. (For interpretation of the references to color in this figure legend, the reader is referred to the web version of this article.)

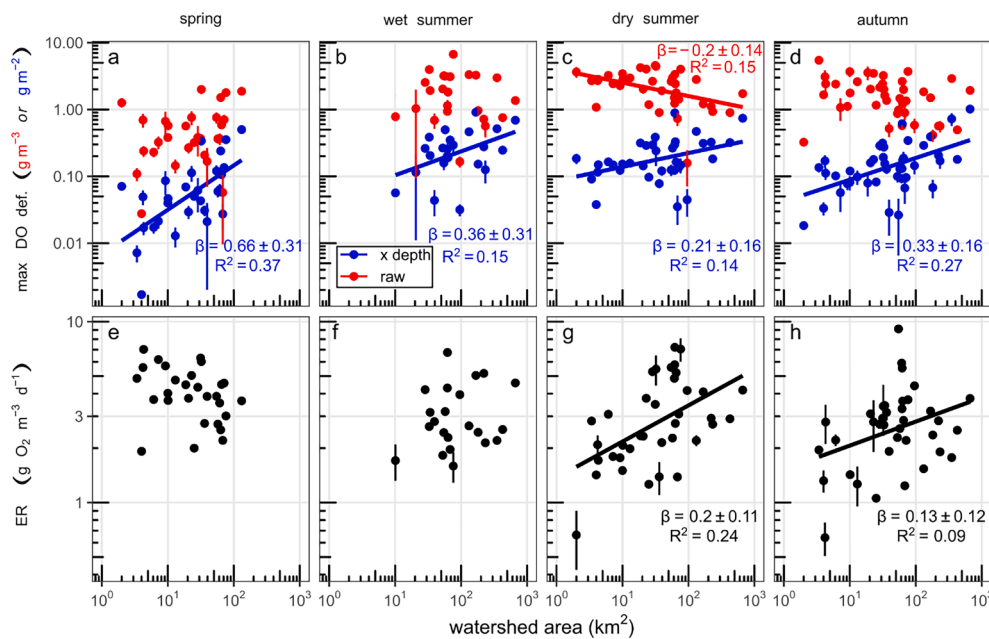


Fig. 6. Spatial patterns in mean daily $|ER|$ and mean maximum daily DO deficit by season and watershed area. a-d) Red points are raw values of maximum daily DO deficit and blue points are indexed by stream depth (note change in units on y-axis). e-h) ER diverges from spatial pattern to maximum daily DO deficit \times depth, except in the dry summer and autumn (g). Vertical bars indicate standard errors; non-visible standard errors are smaller than the plotted point. Best fit lines are ordinary least square regressions and text indicates ordinary least squares slope coefficients \pm 95% confidence intervals and coefficients of determination (R^2); text and best fit lines only shown for $p < 0.05$. Note log-log scale. (For interpretation of the references to color in this figure legend, the reader is referred to the web version of this article.)

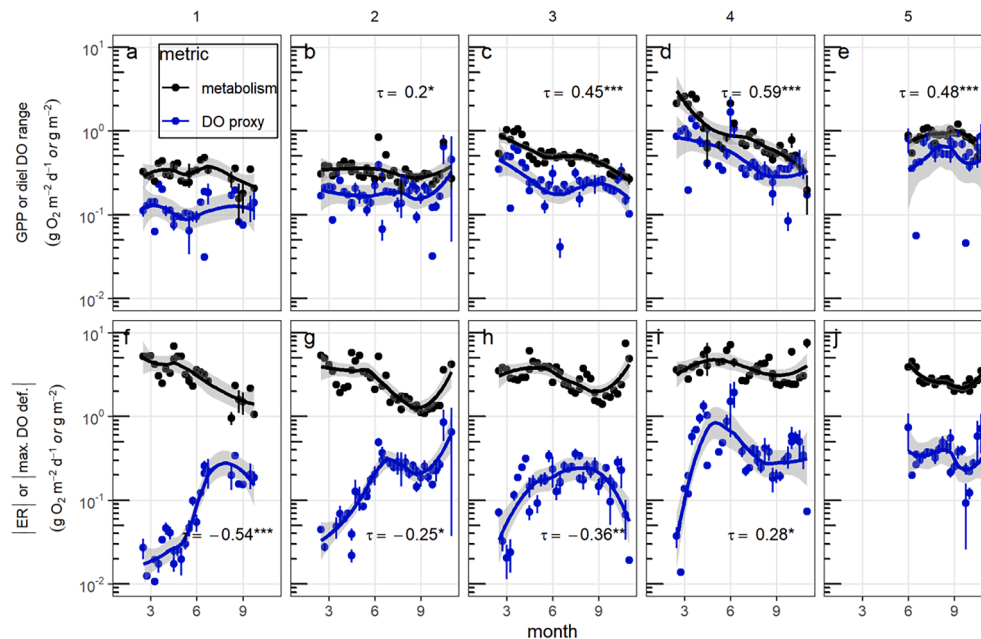


Fig. 7. Weekly time series of metabolism (black points) and DO metrics (blue points) by Strahler order (columns). Temporal patterns in mean diel DO range \times depth correspond with temporal patterns in GPP across Strahler orders (a-e), whereas maximum daily deficit \times depth was anti-correlated with ER for Strahler orders 1–3 (f-j). To visualize temporal patterns, loess fits are shown with shaded confidence intervals. Kendall τ values are shown when $p < 0.05$, and asterisks indicate p -value < 0.05 (*), < 0.01 (**), and < 0.001 (***) $.$ Vertical bars indicate standard errors. Note log y-axis. (For interpretation of the references to color in this figure legend, the reader is referred to the web version of this article.)

uncorrelated with either in the wet summer. Interestingly however, the direction of correlation for the maximum daily DO deficit and S_R differed between the two summers: wet summer S_R decreased with increasing deficit magnitude, while dry summer S_R increased with increasing deficit magnitude (Fig. 8d).

The high values of $\delta^{15}\text{N-NO}_3$ ($11.3 \pm 4.6\text{‰}$; mean \pm sd) and low isotope ratios ($\delta^{18}\text{O}/\delta^{15}\text{N} = 0.38 \pm 0.17$) indicate stream nitrate is derived primarily from animal manure (Kendall, 2012). During winter, $\delta^{15}\text{N-NO}_3$ was constrained across catchments (Fig. 9a). However, during both summers, $\delta^{15}\text{N-NO}_3$ was enriched at all sites compared to winter. The maximum daily DO deficit and $\delta^{15}\text{N-NO}_3$ both peaked during the dry summer, and the relationship between $\delta^{18}\text{O-NO}_3$ and $\delta^{15}\text{N-NO}_3$ followed the characteristic denitrification slope of 0.5 (Fig. 9b). We observed no influence of catchment size or DOC concentration on the distribution of isotopic values ($p > 0.1$). However, NO_3-N was

negatively correlated with $\delta^{15}\text{N-NO}_3$ ($r = -0.48$, $p < 0.001$), as were DOM S_R ($r = -0.68$, $p < 0.001$) and SUVA ($r = -0.5$, $p < 0.001$); E2:E3 was positively correlated with $\delta^{15}\text{N-NO}_3$ ($r = 0.7$, $p < 0.001$). Most importantly, $\delta^{15}\text{N-NO}_3$ was strongly positively correlated with the magnitude of maximum daily DO deficit (Fig. 8c, $F_{45} = 43.1$, $p < 0.001$, $R^2 = 0.49$). In contrast, neither $\delta^{15}\text{N-NO}_3$ nor $\delta^{18}\text{O-NO}_3$ were correlated with ER (Fig. 9d).

4. Discussion

4.1. DO metrics are better proxies of GPP than ER

The allure of DO metrics emerges from their simplicity and applicability in all settings and dates, but our data make clear that while simple DO metrics serve as robust proxies for stream GPP, their

Table 3

Summary of stream grab sample results for DOC and DOM UV-vis (mean \pm sd) for the five study catchments for the winter, dry summer, and wet summer seasons (number of samples).

| Watershed | Season | DOC (mg C L ⁻¹) | S _R (-) | E2: E3 (-) | E4: E6 (-) | SUVA (L mg C ⁻¹ m ⁻¹) |
|-----------|-----------------|-----------------------------|--------------------|---------------|---------------|--|
| Loise | Winter (21) | 4.2 \pm 2.0 | 1.6 \pm 0.1 | 2.6 \pm 0.3 | 1.1 \pm 0.0 | 3.6 \pm 0.9 |
| | Dry summer (13) | 3.9 \pm 1.0 | 2.0 \pm 0.5 | 2.8 \pm 0.3 | 1.1 \pm 0.0 | 4.1 \pm 0.4 |
| | Wet summer (10) | 5.1 \pm 0.9 | 0.9 \pm 0.0 | 5.3 \pm 0.2 | 5.6 \pm 2.0 | 2.7 \pm 0.1 |
| Toranche | Winter (3) | 7.1 \pm 0.9 | 1.4 \pm 0.0 | 3.3 \pm 0.0 | 1.1 \pm 0.0 | 3.1 \pm 0.1 |
| | Dry summer (3) | 5.3 \pm 0.7 | 1.9 \pm 0.2 | 3.1 \pm 0.1 | 1.1 \pm 0.1 | 3.3 \pm 0.2 |
| | Wet summer (3) | 7.6 \pm 2.0 | 0.9 \pm 0.1 | 5.7 \pm 0.0 | 4.7 \pm 2.0 | 2.9 \pm 0.2 |
| Coise | Winter (9) | 4.7 \pm 0.4 | 1.5 \pm 0.1 | 2.9 \pm 0.1 | 1.1 \pm 0.0 | 3.4 \pm 0.1 |
| | Dry summer (9) | 3.6 \pm 0.7 | 1.9 \pm 0.5 | 2.8 \pm 0.3 | 1.1 \pm 0.0 | 4.2 \pm 0.3 |
| | Wet summer (3) | 6.5 \pm 0.8 | 0.9 \pm 0.0 | 5.8 \pm 0.1 | 6.5 \pm 0.7 | 2.6 \pm 0.2 |
| Lignon | Winter (7) | 4.9 \pm 1.0 | 1.4 \pm 0.0 | 2.9 \pm 0.2 | 1.2 \pm 0.0 | 4.0 \pm 0.4 |
| | Dry summer (4) | 5.1 \pm 3.0 | 1.7 \pm 0.2 | 3.0 \pm 0.4 | 1.1 \pm 0.0 | 4.1 \pm 1.0 |
| | Wet summer (4) | 5.4 \pm 2.0 | 0.9 \pm 0.1 | 5.0 \pm 0.1 | 4.7 \pm 2.0 | 3.0 \pm 0.6 |
| Mare | Winter (4) | 7.0 \pm 2.0 | 1.3 \pm 0.2 | 3.2 \pm 0.1 | 1.2 \pm 0.1 | 3.9 \pm 0.8 |
| | Dry summer (4) | 8.6 \pm 1.0 | 1.3 \pm 0.2 | 3.6 \pm 0.1 | 1.3 \pm 0.1 | 3.8 \pm 0.2 |
| | Wet summer (4) | 6.2 \pm 0.9 | 1.0 \pm 0.0 | 5.3 \pm 0.4 | 2.8 \pm 0.4 | 3.2 \pm 0.3 |

performance for capturing spatial and temporal variation in ER is far weaker. Specifically, the depth-scaled diel DO range was an excellent proxy for GPP, accounting for 70% of GPP variation (Fig. 4b) throughout the network, capturing both spatial and temporal patterns in stream primary production. Indeed, a multiple regression model that consider stream order interactions suggests that depth-scaled diel DO range is, by itself, sufficient to predict network variation in GPP, with no variation in fitted intercepts or slopes at different stream orders. In contrast, the

Table 4

Comparison of watershed scaling relationships for mean annual stream metabolism fluxes.

| Metabolic flux | slope (std. err.) | range of areas [km ²] (n) | p-value | R ² | Reference |
|----------------|-------------------|---------------------------------------|---------|----------------|-------------------------|
| GPP | 0.30 (0.04) | 2–664 (42) | <0.001 | 0.52 | This paper |
| | 1.46 (0.22) | 128–1722 (10) | <0.001 | 0.84 | (Mejia et al., 2019) |
| | 0.26 (0.06) | 7–17551 (47) | <0.001 | 0.32 | (Savoy et al., 2019) |
| | 0.18 (0.04) | 0.1–6860 (78) | <0.001 | 0.26 | (Finlay, 2011) |
| | 0.54 (0.07) | 0.1–10010 (103) | <0.001 | 0.59 | (Finlay, 2011) |
| | 0.22 (0.07) | 0.8–35900 (8) | 0.02 | 0.64 | (Minshall et al., 1992) |
| ER | 0.01 (0.1) | 2–664 (42) | 0.8 | 0 | This paper |
| | 0.81 (0.15) | 128–1722 (10) | <0.001 | 0.78 | (Mejia et al., 2019) |
| | 0.23 (0.05) | 0.1–6860 (103) | <0.001 | 0.38 | (Finlay, 2011) |
| | 0.03 (0.04) | 0.1–10010 (86) | 0.345 | 0 | (Finlay, 2011) |
| | 0.19 (0.09) | 0.8–35900 (8) | 0.08 | 0.43 | (Minshall et al., 1992) |

*The two slopes in this reference correspond to “natural” (1st line) and human-dominated systems (2nd line). No information was given on the overall fit across system types.

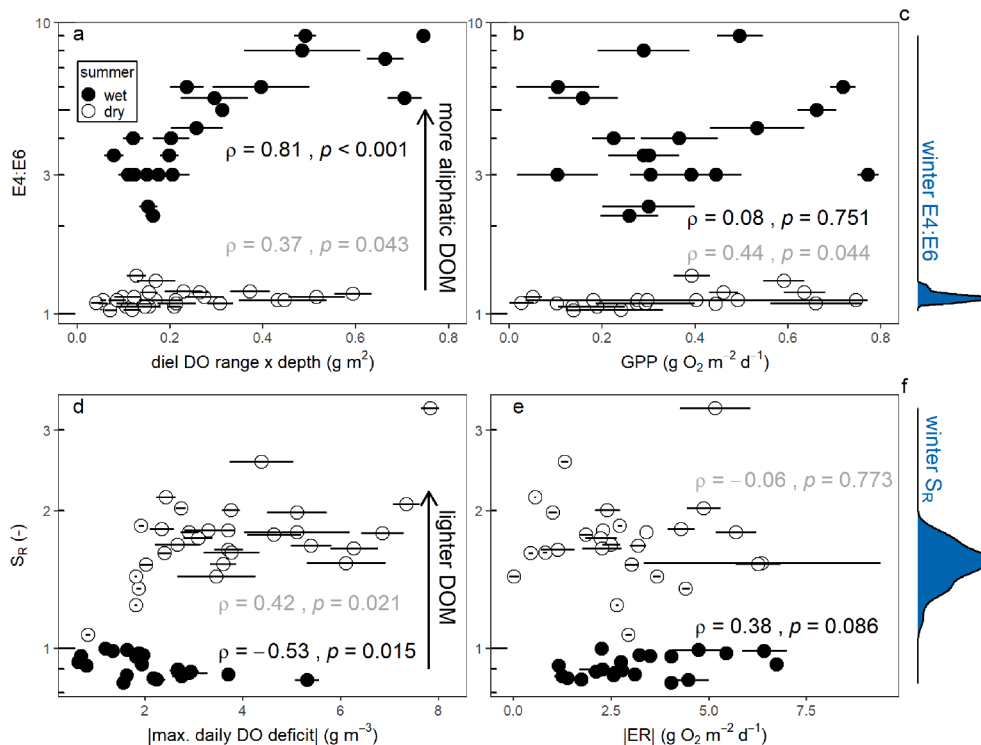


Fig. 8. Relationship between DO metrics and UV-vis of DOM from grab samples collected in the wet summer, dry summer, and winter across the five watersheds. a) E4: E6 versus mean diel DO range \times depth; higher values of E4:E6 typically indicate more aliphatic DOM compounds. b) E4:E6 versus GPP. c) Kernel density plot of E4:E6 values for winter grab samples (February 2020); y-scale is the same as in (a) and (b). d) S_R versus mean maximum daily DO deficit; note flipped x-axis. Higher S_R values typically indicate lower molecular weight DOM. e) S_R versus ER. f) Kernel density plot of winter grab samples for S_R; y-scale is the same as in (d) and (e). Points in a,b,d,e indicate mean values for the three days surrounding grab sample measurement with points filled by summer period (blue = August 2019, red = July 2020) and standard error shown as horizontal error bars. Note log scales on y-axes. Text indicates Spearman's rho and associated p-value. (For interpretation of the references to color in this figure legend, the reader is referred to the web version of this article.)

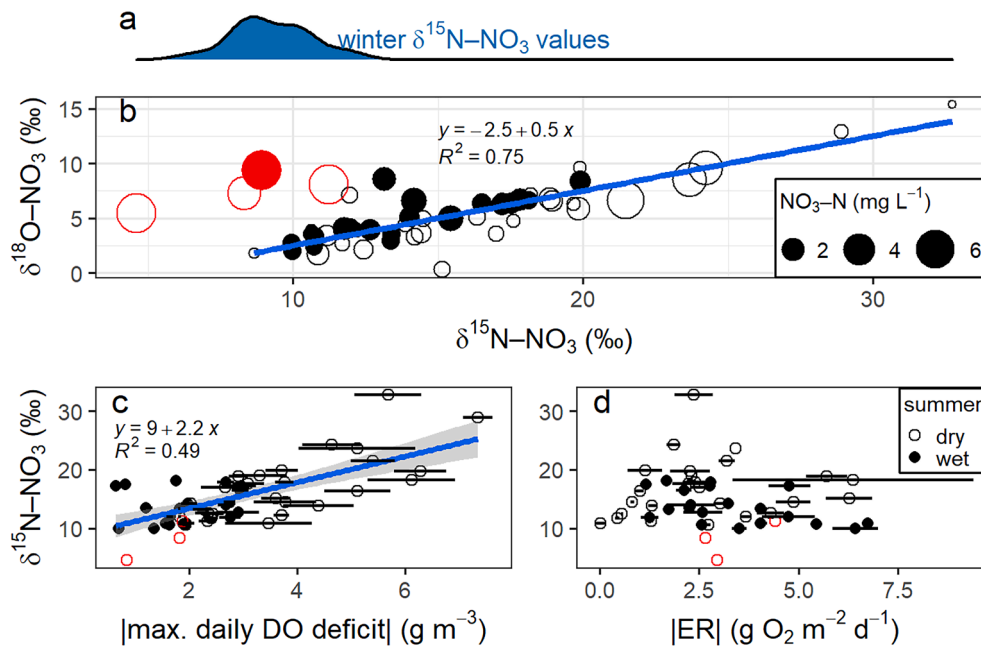


Fig. 9. Nitrate isotopes and their relation to maximum daily DO deficit and ER for the dry and wet summer periods. a) Kernel density plot of $\delta^{15}\text{N-NO}_3$ values for all sites for both winter samples (December 2019 and February 2020) with axis values identical to those in (b). b) $\delta^{18}\text{O-NO}_3$ versus $\delta^{15}\text{N-NO}_3$ with points filled by their season (dark fill = wet summer, no fill = dry summer) and sized by stream $\text{NO}_3\text{-N}$ concentration. The fitted line is a linear regression. Red points indicate samples taken from the Mare watershed that were identified as outliers and not included in the regression. c) $\delta^{15}\text{N-NO}_3$ versus the mean maximum daily DO deficit for the three days surrounding the grab sample; horizontal error bars indicate the standard error for the three days. The fitted line is a linear regression with text reporting regression results. d) $\delta^{15}\text{N-NO}_3$ versus the mean ER for the three days surrounding the grab sample; horizontal error bars indicate the standard error for the three days.

maximum daily DO deficit (with and without depth-scaling) was a poor proxy for ER, exhibiting limited predictive power (<10% of ER variation explained), except in higher order streams (Fig. 4c,d). Notably, while its global ER predictions were weak, this DO metric did capture key aspects of network variation, with systematically increasing depth-scaled DO deficits in higher order streams (monotonic changes in fitted intercepts with increasing order in Table 2), and increasing fitted slopes for orders 2 through 5, indicating that greater DO deficits imply increasing ER in larger rivers.

Our general finding that DO metrics require depth-adjustment to be effective does not comport with results in Mulholland et al. (2005) who observed no improvement in the association between GPP and the DO diel range with depth adjustment. That study also reported clear relationships between ER and maximum DO deficit, in stark contrast to our findings. This discrepancy is likely attributable to the larger range of catchment areas in our study ($1\text{--}664 \text{ km}^2$ vs $0.3\text{--}3.7 \text{ km}^2$) with attendant greater range in stream physical attributes (e.g., depth, gas exchange). We note that within any given order, the GPP vs. diel DO range relationship is very strong (Fig. 4a) but with contrasting slopes for different stream orders. We also note the DO proxies used in Mulholland et al. (2005) were strongly predicted by drainage area disturbance, a finding our observations failed to replicate, possibly because of the comparative severity and ubiquity of human impacts in our catchments (Fig. S3).

Our finding of global utility for depth-scaled diel DO range, but order-specific utility for depth-scaled maximum DO daily deficit implies two possible conclusions. First, temporal variation in DO is nearly entirely due to GPP, with this relationship only weakly influenced by spatial scale (increasing R^2_{adj} by 3% when considering order effects). The unexplained variation in this proxy relationship (~25%) may be attributed to measurement error or site-specific conditions like local re-aeration hotspots that erase GPP signals. The second conclusion is that ER is poorly constrained, especially in low order streams (Fig. 4d), where rapid gas exchange (Fig. 3a) can induce equifinality in ER and K_{600} estimates when diel ranges are small. In higher order streams, the depth-scaled maximum daily DO deficit served as a reasonable proxy for ER (e.g., in 5th order streams, we observed $R^2 = 0.54$, $\beta = 2.1$, $F_{1,469} = 557$, $p < 0.001$). Moreover, ER may be more strongly influenced than GPP by local heterogeneity in stream properties such as relative distributions of pools, eddies, DOM quality, and inflows of limiting nutrients and carbon sources from confluences and groundwater (Lupon et al.,

2019).

4.2. Clear network patterns for GPP, but not ER

Our results strongly support predictable network patterns of stream GPP in agricultural headwaters, and further support the use of diel DO range as a proxy for that spatial network variation. GPP clearly increases with catchment size (Fig. 5), with the scaling of this increase aligned closely with concomitant patterns in depth-scaled diel DO range (Fig. 5a-d). The most plausible explanation for this is increasing light availability with increasing stream order and width. Indeed, GPP exhibited positive relationships with stream surface light availability for all stream orders, with regression intercepts increasing with order (consistent with Kirk et al. 2020; Fig. S2). We estimated light use efficiency as the ratio of GPP and stream light availability (after both are normalized to $\text{kJ m}^{-2} \text{ d}^{-1}$ using methods from Kirk et al. 2020), and found it to range from 0.06 to 1.4% (mean = 0.5%), considerably lower than those observed in (Kirk et al., 2020), which were closer to 2–3%. We attribute this to large light reduction effects of geomorphic shading (Fig. S4) and water depth, reflectance, and color that were not taken into account.

In contrast, ER exhibited no clear trends with watershed size (Fig. 6), in agreement with previous work indicating complex, non-monotonic change in ER through river networks (cf. Battin et al., 2008; Hotchkiss et al., 2015). Substantial spatial heterogeneity in ER was matched by the depth-adjusted maximum daily DO deficit, which exhibited similar order-of-magnitude network variation within each season (Fig. 6a-d). We note, however, that uncertainties in ER estimates were large (3–4 times those for GPP), and its estimates were considered poor for 54% of days, challenging strong inference on ER spatial patterns. Using the DO deficit metric instead, we observe a clear network pattern aligned with the patterns observed for GPP (Fig. 6a-d). Indeed, if we take the DO deficit metric as a reasonable proxy for ER, the patterns observed suggest that ER increased at rates similar to GPP along the river network. This should be expected given the importance of autotrophic respiration to ER in headwater networks (Segatto et al., 2021).

While GPP increased nearly an order-of-magnitude through our study networks, the contribution of small streams to GPP at the whole network scale was larger. Using mean GPP by Strahler order for every reach across all five watersheds, and scaling for variation in benthic

surface area (m^2), leads to the estimate that Strahler orders 1–3 produced $81 \pm 2\%$ more DO than Strahler orders 4–5 (in $\text{g O}_2 \text{ d}^{-1}$). Given that low order streams represent 76% of total stream benthic area, this result indicates that cumulative river network GPP is dominated by headwaters, which aligns well with recent theoretical modeling (Koenig et al., 2019). We further estimate that benthic area-scaled ER ($\text{g O}_2 \text{ d}^{-1}$) was $337 \pm 2\%$ higher in orders 1–3 than orders 4–5. This far more dramatic importance of low-order streams in networks suggests that these reaches are hotspots for internally derived CO_2 efflux to the atmosphere. Yet, we cannot determine the importance of this source in relation to terrestrial derived CO_2 , which is typically considered larger in headwaters (Hotchkiss et al., 2015).

Depth adjustments to our DO metrics were critical for producing network-scale DO patterns that resemble those from metabolism. Indeed, the patterns of non-depth-scaled DO metrics with increasing watershed area were ambiguous for much of the year (Fig. 5a–d), while depth scaling led to consistent spatial patterns. This underscores the dominant role of stream depth on benthic (i.e. 2-dimensional) processes altering water column (i.e., 3-dimensional) DO concentrations, much like the reasoning of surface area to volume ratio for explaining disproportionate reactivity of headwater streams (Alexander et al., 2000). Hence, as depth increases downstream, DO signals should dampen under the same metabolic fluxes. On the other hand, atmospheric gas exchange tends to decrease downstream as slopes and velocities diminish in higher orders (Raymond et al., 2012), which amplifies the DO signals driven by metabolic fluxes. Hence, there are two opposing physical drivers controlling DO network patterns in the downstream direction: 1) an increasing depth-effect that reduces DO response to areal fluxes, and 2) a decreasing gas-exchange effect that increases DO response to areal fluxes. This implies that with constant stream network metabolism, the balance between these hydraulic controls should create spatially constant diel DO ranges through the network. Our observations to the contrary (Figs. 5 and 6) necessarily imply increasing metabolism along the river network (see Fig. S5).

We observed power-law scaling of stream metabolism with watershed area, with scaling exponents typically greater than those for stream depth vs. area in most instances (i.e., $\beta = 0.30\text{--}0.50$ compared to 0.27). This was clearest for GPP across seasons ($\beta = 0.28\text{--}0.52$), and ER in the dry summer and autumn ($\beta = 0.13\text{--}0.20$), although the depth-scaled maximum daily DO deficit also exhibited clear power law scaling across seasons (Figs. 5 and 6). In spring, the fitted exponents for GPP and DO metric vs. area were 93% and 74% greater than the fitted depth vs. area exponents, respectively, clearly indicating a biological DO signal above that expected from hydraulics alone. These scaling values appear to hold remarkably well at larger scales in the Loire River network. Using the fitted scaling function ($\beta = 0.4$ based on the mean of spring and summer), mean growing season GPP in the Loire at Dampierre (watershed area = 35,000 km^2) is predicted to be $7.6 \text{ g O}_2 \text{ m}^{-2} \text{ d}^{-1}$, which is well within the range of recent estimates of $6.2\text{--}8.0 \text{ O}_2 \text{ m}^{-2} \text{ d}^{-1}$ (Diamond et al., n.d.). GPP scaling values in the literature range from 0.2 to 0.5 (Table 4), suggesting convergence in network spatial patterning. Scaling exponents for ER are more variable, but consistently lower than those for GPP (Table 4) and also lower than for depth-area. This likely arises because ER is relatively constant through networks, with GPP:ER scaling behavior emerging as the difference between GPP and ER slopes (0.30 in our case; across site GPP:ER range = 0.06–0.54).

4.3. Temporal patterns in DO metrics and metabolism align, especially in larger streams

Our DO metrics qualitatively captured temporal patterns in stream metabolism, supporting their use as metabolic proxies. As with spatial metabolism patterns, the temporal patterns were best aligned between GPP and depth-scaled diel DO range, which exhibited strong temporal coherence (Kendall $\tau > 0.2$) for stream orders 2–5 (Fig. 7a–d). This result further supports that depth adjusted diel DO range can effectively

capture GPP regimes (Bernhardt et al., 2018), with our streams exhibiting the “spring peak” productivity regime (Savoy et al., 2019). In contrast, ER was temporally aligned with depth adjusted maximum daily DO deficit only in stream order 4 (though $p = 0.06$ in stream order 5, Fig. 7j). Surprisingly, our temporal patterns in this DO proxy were negatively-correlated with ER for low order streams, suggesting contrasting information content regarding in-stream functioning in network headwaters. All interpretations of ER patterns are perilous, especially in our lower order reaches, because of significant uncertainties and equifinality in the *streamMetabolizer* estimates (Fig. S1). When we consider effects of temperature variation (Figs. S6), which can impact ER far more than GPP (Song et al., 2018), we observe a counterintuitive inverse pattern for our ER estimates, but a clear and theoretically compelling temperature effect on the depth adjusted maximum deficit ($\beta = 0.02$, $R^2 = 0.90$, $p < 0.001$; Fig. S7). Given the known positive thermal control on ER (Allen et al., 2005; Demars et al., 2011; Yvon-Durocher et al., 2012), our results indicate that when stream metabolism is poorly estimated, as we observe most acutely in our headwater streams, DO metrics may provide complementary utility for inferring spatiotemporal patterns in ecosystem processes.

4.4. DO metrics outperform metabolic rates for inferring stream DOM quality and denitrification

In line with our expectations, DO metrics consistently outperformed metabolism in inferring DOM quality (i.e., weight, size, and aromaticity) and denitrification (inferred from $\delta^{15}\text{N-NO}_3^-$ enrichment patterns) (Fig. 8). Aliphatic content of DOM was highest with high GPP (Fig. 8ab), but the depth-scaled DO diel range provided a more consistent predictor than GPP across the two summer periods (Fig. 8a). Contrary to our expectations of lighter DOM molecules with increasing ER, we observed strong seasonally contrasting patterns between depth-scaled maximum DO deficit (our ER proxy) and S_R (Fig. 8c), which corresponds to DOM molecular weight (Helms et al., 2008). Only during the dry summer did DOM molecular weight decrease (S_R increase) with increasing DO deficits as expected; during the wet season this pattern was reversed, albeit changes in S_R were small (Fig. 8d).

The high values of S_R (e.g., >2) in the dry summer are atypical in flowing freshwater systems (Hansen et al., 2016; Hosen et al., n.d.). However, the striking contrast in S_R (Fig. 8c), E4:E6 (Fig. 8a), SUVA, and E2:E3 (Table 4) between the wet and dry summer periods has some precedent in other drying systems (Guarch-Ribot and Butturini, 2016). Moreover, the strong similarity in DOM quality metrics between dry summer values and winter values suggests a common DOM source that is distinct from the wet summer. During the dry summer, we observed clear and cool water at our sites (Fig. S5), indicative of deeper groundwater inputs. Previous work suggest that S_R values like those we observed may imply a groundwater source for both dry summer and winter samples (Messelha et al., 2018), although other biological interactions may be involved, complicating interpretations (Guarch-Ribot and Butturini, 2016; Harjung et al., 2018). This source effect is likely to override the importance of internal processes affecting DOM, although we also note that dry summer S_R values are similar to those observed in highly irradiated systems (Helms et al., 2008). Thus, the observed S_R signals for the dry summer could also result from increasing hydrologic disconnection, pool formation, and increased light exposure.

The maximum daily DO deficit strongly covaried with denitrification proxies in our catchments, explaining nearly 50% of the variation in $\delta^{15}\text{N-NO}_3^-$. In contrast, ER was uncorrelated with stable isotopes of NO_3^- (Fig. 9d), as was the depth-scaled maximum daily DO deficit ($F_{45} = 0.27$, $p = 0.606$). This finding suggests that water column DO concentration closely reflects denitrification potential in flowing water systems. The poor performance of ER as a covariate of denitrification likely arises because ER estimates partially obscure site information about ambient DO concentration, which ultimately controls the favourability of this particular N reaction pathway. Further, denitrification, and likely all

other stream anaerobic reactions, are likely to have small effects compared to aerobic reactions that comprise oxygen-derived measurements of ER (Mulholland et al., 2009). As such, the linear relationship between $\delta^{15}\text{N-NO}_3^-$ and the maximum DO deficit may arise as a consequence of high NO_3^- availability in this agricultural catchment (Kreiling et al., 2019), and further, it suggests that denitrification in these N-enrich flowing waters was progressive rather than an abrupt process.

4.5. Benefits of DO metrics as metabolism proxies

Scientists, government agencies, and stakeholders are increasingly turning to high-resolution DO data to understand, regulate, and manage freshwater resources (Jankowski et al., 2021). This alone animates the utility of simple DO metrics that balance the competing requirements of information density, uncertainty, and computational complexity. Building on previous efforts (Moatar et al., 2001; Mulholland et al., 2005; Wang et al., 2003), we suggest that two simple DO proxies for ecosystem metabolism - the diel range and the maximum daily DO deficit - can inform large scale patterns of GPP and ER along river networks. We show that these metrics reveal similar spatiotemporal patterns, and even similar magnitudes for GPP (Fig. 3). In addition to the strong spatial and temporal concordance between metabolism and these DO metrics, their advantages are multiple. They allow use of the entirety of recorded DO datasets, foregoing the frustrating data losses normally associated with metabolism measurements (60–70% in our study). They are simple and require no specialized inference tools, rendering them more widely applicable. They align directly with existing water quality protection frameworks. And finally, they are more directly informative than metabolism about DOM quality and denitrification potential in small stream networks. When conditions are sub-optimal for metabolism estimates, such as storm events or low flow periods, and reaches with high groundwater inputs or near confluences, these DO metrics provide useful inference tools for managers. Our results make clear that while estimating stream metabolism wherever possible is a foundational facet of river network ecosystem science, the use of simple DO metrics captures much of the meaningful information about space and time variation with far fewer assumptions and yields important insights on biogeochemical controls. These metrics can and should be an important complement in our efforts to use increasingly massive sensor data sets to effectively characterize flowing water systems.

CRediT authorship contribution statement

Jacob S. Diamond: Conceptualization, Methodology, Software, Formal analysis, Investigation, Data curation, Writing – original draft, Writing - review & editing, Visualization. **Susana Bernal:** Conceptualization, Writing – original draft, Writing - review & editing. **Amine Boukra:** Resources. **Matthew J. Cohen:** Conceptualization, Writing – original draft, Writing - review & editing. **David Lewis:** Methodology, Investigation, Writing - review & editing. **Matthieu Masson:** Resources. **Florentina Moatar:** Conceptualization, Supervision, Funding acquisition, Project administration, Writing - review & editing. **Gilles Pinay:** Conceptualization, Methodology, Investigation, Supervision, Writing – original draft, Writing - review & editing.

Declaration of Competing Interest

The authors declare that they have no known competing financial interests or personal relationships that could have appeared to influence the work reported in this paper.

Acknowledgements

This study was supported by the Agence de l'Eau Loire-Bretagne, the Agence de l'eau Rhône-Méditerranée-Corse and the EUR H2O'Lyons. SB

work was supported by a RyC fellowship (RYC-2017-22643) from the Spanish Government and AEI/FEDER UE. We would like to thank Ilyes and Imran Amraoui-Pinay for their help in the field work on the Charnassonne and Loise streams. We would also like to thank Restaurant Le Chaudron in Feurs, Ma Campagne in Jas, and Restaurant Le Nezel in Larajasse for providing comfort and hospitality during field work.

Appendix A. Supplementary data

Supplementary data to this article can be found online at <https://doi.org/10.1016/j.ecolind.2021.108233>.

References

Alexander, R.B., Smith, R.A., Schwarz, G.E., 2000. Effect of stream channel size on the delivery of nitrogen to the Gulf of Mexico. *Nature* 403, 758–761. <https://doi.org/10.1038/35001562>.

Allen, A.P., Gillooly, J.F., Brown, J.H., 2005. Linking the global carbon cycle to individual metabolism. *Funct. Ecol.* 19, 202–213.

Appling, A.P., Hall, R.O., Yackulic, C.B., Arroita, M., 2018. Overcoming equifinality: leveraging long time series for stream metabolism estimation. *J. Geophys. Res. Biogeosci.* 123, 624–645. <https://doi.org/10.1002/2017JG004140>.

Battin, T.J., Kaplan, L.A., Findlay, S., Hopkinson, C.S., Marti, E., Packman, A.I., Newbold, J.D., Sabater, F., 2008. Biophysical controls on organic carbon fluxes in fluvial networks. *Nat. Geosci.* 1, 95–100.

Beaufort, A., Curie, F., Moatar, F., Ducharme, A., Melin, E., Thierry, D., 2016. T-NET, a dynamic model for simulating daily stream temperature at the regional scale based on a network topology. *Hydrolog. Process.* 30, 2196–2210.

Bernhardt, E.S., Heffernan, J.B., Grimm, N.B., Stanley, E.H., Harvey, J.W., Arroita, M., Appling, A.P., Cohen, M.J., McDowell, W.H., Hall, R.O., Read, J.S., Roberts, B.J., Stets, E.G., Yackulic, C.B., 2018. The metabolic regimes of flowing waters: Metabolic regimes. *Limnol. Oceanogr.* 63, S99–S118. <https://doi.org/10.1002/lno.10726>.

Blaszcak, J.R., Delesantro, J.M., Urban, D.L., Doyle, M.W., Bernhardt, E.S., 2019. Scoured or suffocated: Urban stream ecosystems oscillate between hydrologic and dissolved oxygen extremes. *Limnol. Oceanogr.* 64, 877–894.

Brooks, S.P., Gelman, A., 1998. General methods for monitoring convergence of iterative simulations. *J. Comput. Graph. Statistics* 7, 434–455.

Casciotti, K.L., Sigman, D.M., Hastings, M.G., Böhlke, J.K., Hilkert, A., 2002. Measurement of the oxygen isotopic composition of nitrate in seawater and freshwater using the denitrifier method. *Anal. Chem.* 74, 4905–4912.

Christensen, P.B., Nielsen, L.P., Sørensen, J., Revsbech, N.P., 1990. Denitrification in nitrate-rich streams: Diurnal and seasonal variation related to benthic oxygen metabolism. *Limnol. Oceanogr.* 35, 640–651.

Cubizolle, H., Fassion, F., Argant, J., Latour-Argant, C., Galet, P., Oberlin, C., 2012. Mire initiation, climatic change and agricultural expansion over the course of the Late-Holocene in the Massif Central mountain range (France): Causal links and implications for mire conservation. *Quaternary International*, LAC 2010: 1st international conference on Landscape Archaeology 251, 77–96. <https://doi.org/10.1016/j.quaint.2011.07.001>.

Cubizolle, H., Tourman, A., Argant, J., Portet, J., Oberlin, C., Serieyssol, K., 2003. Origins of European biodiversity: palaeo-geographic signification of peat inception during the Holocene in the granitic eastern Massif Central (France). *Landscape Ecol.* 18, 227–238.

Demars, B.O., Russell Manson, J., Olafsson, J.S., Gislason, G.M., Gudmundsdottir, R., Woodward, G.U.Y., Reiss, J., Pichler, D.E., Rasmussen, J.J., Friberg, N., 2011. Temperature and the metabolic balance of streams. *Freshwater Biol.* 56, 1106–1121.

Demars, B.O.L., Thompson, J., Manson, J.R., 2015. Stream metabolism and the open diel oxygen method: Principles, practice, and perspectives: Problems in stream metabolism studies. *Limnol. Oceanogr. Methods* 13, 356–374. <https://doi.org/10.1002/lim3.10030>.

Diamond, J.S., Moatar, F., Cohen, M.J., Poirel, A., Martinet, C., Maire, A., Pinay, G., n.d. Metabolic regime shifts and ecosystem state changes are decoupled in a large river. *Limnology and Oceanography* n/a. <https://doi.org/10.1002/lno.11789>.

Finlay, J.C., 2011. Stream size and human influences on ecosystem production in river networks. *Ecosphere* 2, art87. <https://doi.org/10.1890/ES11-00071.1>.

Gelman, A., Rubin, D.B., 1992. Inference from iterative simulation using multiple sequences. *Statistical Sci.* 7, 457–472.

Georges, V., Verrier, J., Cubizolle, H., 2004. Occupation humaine et dynamique fluviale de la Loire en Forez, du Néolithique à l'époque gallo-romaine (France, 42). Occupation, gestion et paléoenvironnement des plaines alluviales de l'âge du Fer à l'Antiquité, Presses Universitaires Franc-Comtoises, Annales Littéraires, Série "Environnement, sociétés et archéologie" 10, 121e134.

Granger, J., Sigman, D.M., 2009. Removal of nitrite with sulfamic acid for nitrate N and O isotope analysis with the denitrifier method. *Rapid Commun. Mass Spectrometry* 23, 3753–3762.

Guarch-Ribot, A., Butturini, A., 2016. Hydrological conditions regulate dissolved organic matter quality in an intermittent headwater stream. From drought to storm analysis. *Sci. Total Environ.* 571, 1358–1369.

Hansen, A.M., Kraus, T.E.C., Pellerin, B.A., Fleck, J.A., Downing, B.D., Bergamaschi, B.A., 2016. Optical properties of dissolved organic matter (DOM): effects of biological and photolytic degradation. *Limnol. Oceanogr.* 61, 1015–1032. <https://doi.org/10.1002/lno.10270>.

Harjung, A., Sabater, F., Butturini, A., 2018. Hydrological connectivity drives dissolved organic matter processing in an intermittent stream. *Limnologica* 68, 71–81.

Helms, J.R., Stubbins, A., Ritchie, J.D., Minor, E.C., Kieber, D.J., Mopper, K., 2008. Absorption spectral slopes and slope ratios as indicators of molecular weight, source, and photobleaching of chromophoric dissolved organic matter. *Limnol. Oceanogr.* 53, 955–969.

Hosen, J.D., Allen, G.H., Amatuli, G., Breitmeyer, S., Cohen, M.J., Crump, B.C., Lu, Y.H., Payet, J.P., Poulin, B.A., Stubbins, A., n.d. River network travel time is correlated with dissolved organic matter composition in rivers of the contiguous United States. *Hydrological Processes* e14124.

Hotchkiss, E.R., Hall Jr, R.O., Sponseller, R.A., Butman, D., Klaminder, J., Laudon, H., Rosvall, M., Karlsson, J., 2015. Sources of and processes controlling CO₂ emissions change with the size of streams and rivers. *Nature Geosci.* 8, 696–699. <https://doi.org/10.1038/ngeo2507>.

Jankowski, R.J., Mejia, F.H., Blaszcak, J.R., Holtgrive, G.W., 2021. Aquatic ecosystem metabolism as a tool in environmental management. *Wiley Interdisciplinary Rev.: Water* 8, e1521.

Kendall, C., 2012. Tracing nitrogen sources and cycling in catchments. In: *Isotope Tracers in Catchment Hydrology*. Elsevier, pp. 519–576.

Kirk, L., Hensley, R.T., Savoy, P., Heffernan, J.B., Cohen, M.J., 2020. Estimating benthic light regimes improves predictions of primary production and constrains light-use efficiency in streams and rivers. *Ecosystems* 24. <https://doi.org/10.1007/s10021-020-00552-1>.

Koenig, L.E., Helton, A.M., Savoy, P., Bertuzzo, E., Heffernan, J.B., Hall, R.O., Bernhardt, E.S., 2019. Emergent productivity regimes of river networks. *Limnol. Oceanogr. Lett.* 4, 173–181.

Kreiling, R.M., Richardson, W.B., Bartsch, L.A., Thoms, M.C., Christensen, V.G., 2019. Denitrification in the river network of a mixed land use watershed: unpacking the complexities. *Biogeochemistry* 143, 327–346.

Li, G., Jackson, C.R., Krasiski, K.A., 2012. Modeled riparian stream shading: agreement with field measurements and sensitivity to riparian conditions. *J. Hydrol.* 428, 142–151.

Li, P., Hur, J., 2017. Utilization of UV-Vis spectroscopy and related data analyses for dissolved organic matter (DOM) studies: a review. *Crit. Rev. Environ. Sci. Technol.* 47, 131–154.

Lupon, A., Denfeld, B.A., Laudon, H., Leach, J., Karlsson, J., Sponseller, R.A., 2019. Groundwater inflows control patterns and sources of greenhouse gas emissions from streams. *Limnol. Oceanogr.* 64, 1545–1557.

McTammany, M.E., Webster, J.R., Benfield, E.F., Neatrou, M.A., 2003. Longitudinal patterns of metabolism in a southern Appalachian river. *J. North Am. Benthol. Soc.* 22, 359–370.

Mejia, F.H., Fremier, A.K., Benjamin, J.R., Bellmore, J.R., Grimm, A.Z., Watson, G.A., Newsom, M., 2019. Stream metabolism increases with drainage area and peaks asynchronously across a stream network. *Aquat. Sci.* 81, 9. <https://doi.org/10.1007/s00027-018-0606-z>.

Messetta, M.L., Hegoburu, C., Casas-Ruiz, J.P., Butturini, A., Feijoó, C., 2018. Characterization and qualitative changes in DOM chemical characteristics related to hydrologic conditions in a Pampean stream. *Hydrobiologia* 808, 201–217.

Minshall, G.W., Petersen, R.C., Bott, T.L., Cushing, C.E., Cummins, K.W., Vannote, R.L., Sedell, J.R., 1992. Stream ecosystem dynamics of the Salmon River, Idaho: an 8th-order system. *J. North Am. Benthol. Soc.* 11, 111–137.

Moatar, F., Miquel, J., Poirel, A., 2001. A quality-control method for physical and chemical monitoring data. Application to dissolved oxygen levels in the river Loire (France). *J. Hydrol.* 252, 25–36. [https://doi.org/10.1016/S0022-1694\(01\)00439-5](https://doi.org/10.1016/S0022-1694(01)00439-5).

Morel, M., Booker, D.J., Gob, F., Lamouroux, N., 2020. Intercontinental predictions of river hydraulic geometry from catchment physical characteristics. *J. Hydrol.* 582, 124292. <https://doi.org/10.1016/j.jhydrol.2019.124292>.

Mulholland, P.J., Hall, R.O., Sobota, D.J., Dodds, W.K., Findlay, S.E.G., Grimm, N.B., Hamilton, S.K., McDowell, W.H., O'Brien, J.M., Tank, J.L., Ashkenas, L.R., Cooper, L.W., Dahm, C.N., Gregory, S.V., Johnson, S.L., Meyer, J.L., Peterson, B.J., Poole, G.C., Valett, H.M., Webster, J.R., Arango, C.P., Beaulieu, J.J., Bernot, M.J., Burgin, A.J., Crenshaw, C.L., Helton, A.M., Johnson, L.T., Niederlehrer, B.R., Potter, J.D., Sheibley, R.W., Thomas, S.M., 2009. Nitrate removal in stream ecosystems measured by 15N addition experiments: denitrification. *Limnol. Oceanogr.* 54, 666–680.

Mulholland, P.J., Houser, J.N., Maloney, K.O., 2005. Stream diurnal dissolved oxygen profiles as indicators of in-stream metabolism and disturbance effects: Fort Benning as a case study. *Ecol. Ind.* 5, 243–252. <https://doi.org/10.1016/j.ecolind.2005.03.004>.

Odum, H.T., 1956. Primary production in flowing waters 1. *Limnol. Oceanogr.* 1, 102–117.

Pellerin, B.A., Stauffer, B.A., Young, D.A., Sullivan, D.J., Bricker, S.B., Walbridge, M.R., Clyde, G.A., Shaw, D.M., 2016. Emerging tools for continuous nutrient monitoring networks: sensors advancing science and water resources protection. *JAWRA J. Am. Water Resour. Assoc.* 52, 993–1008.

Poisvert, C., Curie, F., Moatar, F., 2017. Annual agricultural N surplus in France over a 70-year period. *Nutr. Cycl. Agroecosyst.* 107, 63–78.

R Core Team, 2020. R: A Language and Environment for Statistical Computing. R Foundation for Statistical Computing, Vienna, Austria.

Raymond, P.A., Zappa, C.J., Butman, D., Bott, T.L., Potter, J., Mulholland, P., Laursen, A.E., McDowell, W.H., Newbold, D., 2012. Scaling the gas transfer velocity and hydraulic geometry in streams and small rivers: Gas transfer velocity and hydraulic geometry. *Limnol. Oceanogr.* 2, 41–53. <https://doi.org/10.1215/21573689-1597669>.

Roberts, B.J., Mulholland, P.J., Hill, W.R., 2007. Multiple scales of temporal variability in ecosystem metabolism rates: results from 2 years of continuous monitoring in a forested headwater stream. *Ecosystems* 10, 588–606.

Rode, M., Wade, A.J., Cohen, M.J., Hensley, R.T., Bowes, M.J., Kirchner, J.W., Arhonditsis, G.B., Jordan, P., Kronvang, B., Halliday, S.J., Skeffington, R.A., Rozemeijer, J.C., Albert, A.H., Rinke, K., Jomaa, S., 2016. Sensors in the stream: the high-frequency wave of the present. *Environ. Sci. Technol.* 50, 10297–10307. <https://doi.org/10.1021/acs.est.6b02155>.

Savoy, P., Appling, A.P., Heffernan, J.B., Stets, E.G., Read, J.S., Harvey, J.W., Bernhardt, E.S., 2019. Metabolic rhythms in flowing waters: an approach for classifying river productivity regimes. *Limnol. Oceanogr.* 64, 1835–1851.

Segatto, P.L., Battin, T.J., Bertuzzo, E., 2021. The metabolic regimes at the scale of an entire stream network unveiled through sensor data and machine learning. *Ecosystems* 1–18.

Siders, A.C., Larson, D.M., Rüegg, J., Dodds, W.K., 2017. Probing whole-stream metabolism: influence of spatial heterogeneity on rate estimates. *Freshw. Biol.* 62, 711–723.

Sigman, D.M., Casciotti, K.L., Andreani, M., Barford, C., Galanter, M., Böhlke, J.K., 2001. A bacterial method for the nitrogen isotopic analysis of nitrate in seawater and freshwater. *Anal. Chem.* 73, 4145–4153.

Song, C., Dodds, W.K., Riegg, J., Argerich, A., Baker, C.L., Bowden, W.B., Douglas, M.M., Farrell, K.J., Flinn, M.B., Garcia, E.A., Helton, A.M., Harms, T.K., Jia, S., Jones, J.B., Koenig, L.E., Kominoški, J.S., McDowell, W.H., McMaster, D., Parker, S.P., Rosemond, A.D., Ruffing, C.M., Sheehan, K.R., Trentman, M.T., Whiles, M.R., Wollheim, W.M., Ballantyne, F., 2018. Continental-scale decrease in net primary productivity in streams due to climate warming. *Nat. Geosci.* 11, 415–420. <https://doi.org/10.1038/s41561-018-0125-5>.

Vannote, R.L., Minshall, G.W., Cummins, K.W., Sedell, J.R., Cushing, C.E., 1980. The river continuum concept. *Can. J. Fish. Aquat. Sci.* 37, 130–137. <https://doi.org/10.1139/f80-017>.

Wang, H., Hondzo, M., Xu, C., Poole, V., Spacie, A., 2003. Dissolved oxygen dynamics of streams draining an urbanized and an agricultural catchment. *Ecol. Model.* 160, 145–161. [https://doi.org/10.1016/S0304-3800\(02\)00324-1](https://doi.org/10.1016/S0304-3800(02)00324-1).

Weishaar, J.L., Aiken, G.R., Bergamaschi, B.A., Fram, M.S., Fujii, R., Mopper, K., 2003. Evaluation of specific ultraviolet absorbance as an indicator of the chemical composition and reactivity of dissolved organic carbon. *Environ. Sci. Technol.* 37, 4702–4708.

Yvon-Durocher, G., Caffrey, J.M., Cescatti, A., Dossena, M., Giorgio, P.D., Gasol, J.M., Montoya, J.M., Pumpanen, J., Staehr, P.A., Trimmer, M., Woodward, G., Allen, A.P., 2012. Reconciling the temperature dependence of respiration across timescales and ecosystem types. *Nature* 487, 472–476.

Zhang, Y., Liu, X., Wang, M., Qin, B., 2013. Compositional differences of chromophoric dissolved organic matter derived from phytoplankton and macrophytes. *Org. Geochem.* 55, 26–37.